Applications of Digital-Image-Correlation Techniques to Experimental Mechanics

by T.C. Chu, W.F. Ranson, M.A. Sutton and W.H. Peters

Introduction

Optical measurements of macroscopic parameters, such as strain and displacement, have evolved into an accepted branch of experimental stress analysis. Topics such as holography,[1,2] speckle interferometry,[3] speckle photography,[4-6] speckle-shearing interferometry,[7] white-light speckle[8] and moiré[9,10] have advanced from the basic research stage into mature methods employed to analyze a variety of engineering problems.

However, all of these techniques suffer from two major limitations. First, they have varying stability requirements. All interferometric methods have stringent stability requirements which limit their applicability to research environments for most cases. Speckle photography, moiré and white-light speckle have less stringent requirements than those for interferometric techniques, and are more adaptable to industrial applications. Secondly, the data processing required to reduce the fringe patterns and thereby obtain the desired data is laborious and time consuming for each method noted above. However, many researchers have recognized this difficulty and have developed computerized procedures to simplify the data-reduction process. Mendenhall[11] developed a completely automated process to digitize both isopachic and isochromatic fringe patterns, compute fringe numbers, determine partial fringe values and finally output profiles of constant principal-stress values.

More recently, a completely automated approach for the computation of surface strains and displacements was proposed[12] and later employed to determine the center-line displacements of a cantilever beam.[13] The work presented here outlines (a) the basic theory of deformation and digital correlation, as well as how they are combined to form the measurement technique, (b) the interpolation methods employed to extend the range of the measurements and (c) four experiments that have been performed to demonstrate the viability of the method for actual measurements.

T.C. Chu (SEM Member) is Assistant Professor, Polytechnic Institute of New York, Department of Mechanics and Aerospace, 333 Jay Street, Brooklyn, NY 11201. W.F. Ranson (SEM Fellow) is Professor, M.A. Sutton (SEM Member) is Assistant Professor and W.H. Peters (SEM Member) is Associate Professor, University of South Carolina, Department of Mechanical Engineering, Columbia, SC 29208.

Original manuscript submitted: November 25, 1983. Final manuscript received: April 9, 1985.

Theory of Deformation for Use in the Correlation Method

Basic Assumption

Consider an object that is illuminated by a light source. The light-intensity patterns reflected from the undeformed and deformed object surfaces are shown in Fig. 1. Intensity patterns $f(x, y)$ and $f^*(x^*, y^*)$ in Fig. 1 correspond to the reflected light from the undeformed and deformed object configurations. Relative to the intensity patterns, $f(x, y)$ and $f^*(x^*, y^*)$, respectively, they are assumed to be in unique, one-to-one correspondence with the respective object surfaces. Therefore, using this basic assumption, one may measure the deformations of small subsets of the image and thereby obtain deformations of small subsets of the actual object surface.

Object Deformations

The theory discussed in this section may be found in many textbooks.[14,15] It is presented here so that the development of the digital-correlation method, for use in experimental mechanics, may be understood.

Consider an object, such as the one shown in Fig. 2. A basic tenet of continuum mechanics is that differentially small line segments such as PQ, with components (dx, dy, dz), remain as differentially small line segment P*Q*, with components (dx^*, dy^*, dz^*) after deformation. In particular, if (u, v, w) denote the components of displacement of an arbitrary point in the x, y, and z directions, respectively, then one can consider that the points P and Q are located at position (x, y, z) and $(x + dx,\ y + dy,\ z + dz)$ prior to deformation. After deformation, the points P and Q move to points P* and Q* with positions:

$$\mathrm{P}^* = (x^*, y^*, z^*) = [x + u(\mathrm{P}),\ y + v(\mathrm{P}),\ z + w(\mathrm{P})]$$

$$\begin{aligned}\mathrm{Q}^* &= (x^* + dx^*,\ y^* + dy^*,\ z^* + dz^*) \\ &= [x + u(\mathrm{Q}) + dx^*,\ y + v(\mathrm{Q}) + dy^*,\ z + w(\mathrm{Q}) + dz^*] \\ &= [x + u(\mathrm{P}) + u(\mathrm{Q}) - u(\mathrm{P}) + dx,\ y + v(\mathrm{P}) \\ &\quad + v(\mathrm{Q}) - v(\mathrm{P}) + dy,\ z + w(\mathrm{P}) + w(\mathrm{Q}) \\ &\quad - w(\mathrm{P}) + dz] \end{aligned} \tag{1}$$

Therefore, the lengths of the vectors PQ and P*Q* are given by:

$$|PQ|^2 = (ds)^2 = dx^2 + dy^2 + dz^2$$
$$|P^*Q^*|^2 = (ds^*)^2 = dx^{*2} + dy^{*2} + dz^{*2} \quad (2)$$

Using eq (1) to deduce that $dx^* = u(Q) - u(P) + dx$, $dy^* = v(Q) - v(P) + dy$ and $dz^* = w(Q) - w(P) + dz$, one can rewrite eq (2) as:

$$|P^*Q^*|^2 = (ds^*)^2 = [u(Q) - u(P) + dx]^2$$
$$+ [v(Q) - v(P) + dy]^2 + [w(Q) - w(P) + dz]^2 \quad (3)$$

A linear Taylor's expansion of the displacement functions about point P yields:

$$u(Q) - u(P) \cong \frac{\partial u}{\partial x} dx + \frac{\partial u}{\partial y} dy + \frac{\partial u}{\partial z} dz \quad (4)$$
$$v(Q) - v(P) \cong \frac{\partial v}{\partial x} dx + \frac{\partial v}{\partial y} dx + \frac{\partial v}{\partial z} dz$$
$$w(Q) - w(P) \cong \frac{\partial w}{\partial x} dx + \frac{\partial w}{\partial y} dy + \frac{\partial w}{\partial z} dz$$

From eq (4), projections of the deformed lengths dx^*, dy^* dz^* are:

$$dx^* \cong \left(1 + \frac{\partial u}{\partial x}\right) dx + \frac{\partial u}{\partial y} dy + \left(\frac{\partial u}{\partial z}\right) dz$$
$$dy^* \cong \frac{\partial v}{\partial x} dx + \left(1 + \frac{\partial v}{\partial y}\right) dy + \frac{\partial v}{\partial z} dz \quad (5)$$
$$dz^* \cong \frac{\partial w}{\partial x} dx + \frac{\partial w}{\partial y} dy + \left(1 + \frac{\partial w}{\partial z}\right) dz$$

The finite-strain-tensor equations typically noted in textbooks can be derived directly from eq (5). For example, if the points P and Q were originally oriented along the x direction, then $dz = dy = 0$ and eq (5) generates the final values of (dx^*, dy^*, dz^*). Thus the strain tensor is equal to the engineering strain as shown in eq (6).

$$\epsilon_{xx} = \frac{|P^*Q^*| - |PQ|}{|PQ|} =$$
$$\frac{\partial u}{\partial x} + \frac{1}{2}\left[\left(\frac{\partial u^2}{\partial x}\right) + \left(\frac{\partial v^2}{\partial x}\right) + \left(\frac{\partial w^2}{\partial x}\right)\right] \quad (6)$$

For use in digital-correlation work, one notes that the observed intensity pattern is a two-dimensional projection of the object onto a plane. Therefore, the form of the finite-strain equation that one would employ to compute the strain is given by:

$$\epsilon_{xx} \cong \frac{\partial u}{\partial x} + \frac{1}{2}\left[\left(\frac{\partial u^2}{\partial x}\right) + \left(\frac{\partial v^2}{\partial x}\right)\right]$$
$$\epsilon_{yy} \cong \frac{\partial v}{\partial y} + \frac{1}{2}\left[\left(\frac{\partial u}{\partial y}\right)^2 + \left(\frac{\partial v}{\partial y}\right)^2\right] \quad (7)$$
$$\epsilon_{xy} \cong \frac{1}{2}\left(\frac{\partial u}{\partial y} + \frac{\partial v}{\partial x}\right) + \frac{1}{2}\left[\frac{\partial u}{\partial x}\frac{\partial u}{\partial y} + \frac{\partial v}{\partial x}\frac{\partial v}{\partial y}\right]$$

Though eq (7) appears relatively general, one should note carefully the assumptions inherent in its use in digital-image processing. First, one must assume that the out-of-plane displacement does not affect the in-plane deformation or displacement of the characteristic intensity surfaces. This is typically true for low transverse magnifications or when the object deformation is predominately in plane; but it is not generally true. Secondly, one must assume that the derivatives of out-of-plane displacement (i.e., $\frac{\partial w}{\partial x}$) are much less than terms like $\partial u/\partial x$ so that this effect may be excluded from eq (7).

Reconstruction of Digitally Recorded Intensity Patterns

Typically, the two intensity patterns shown in Fig. 1 are recorded by a digitizing camera as a first step in the analysis of object deformation. The intensity value at any sensing-element location—known as a pixel (short for picture element)—usually ranges from 0 to 255. A typical array of the digitized values is shown graphically in Fig. 3,

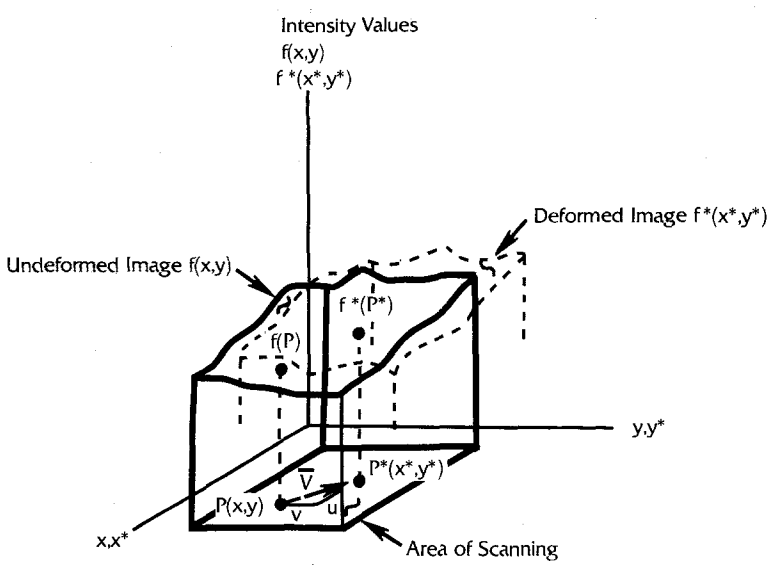

Fig. 1—Gray-level representation of deformed and undeformed digital-speckle images

where the object digitized was coated with a random array of black and white regions to give the 'speckle appearance'. It is noted that random arrays of light and dark regions, such as laser speckle or white-light speckle, were used for all the experimental work to be discussed. This choice was made so that each subset of the image would be statistically different than any other subset. For example, a 10 × 10 subset from Fig. 3 is highlighted in Fig. 4 to indicate its unique intensity variation. Hence, the analyst may look at many small subsets and obtain the local deformation of interest.

Figure 5 shows graphically the discrete form of the intensity data for the 10 × 10 subset highlighted in Fig. 4, as stored in the computer. Since the discrete form is not the most advantageous for this analysis, one would like to reconstruct a more useful model of the intensity pattern. The reasons why the discrete data set is not as advantageous are: (1) the interpolation of values of intensity between pixel location is required for accurate, subpixel displacement calculations and (2) this interpolation is most readily obtained in the computer from an analytic expression for the intensity patterns such as one would obtain by an intensity surface fit. Therefore, if one samples the intensity values at a sufficiently high rate so that the spatial frequency content of the image is not lost, then one may interpolate between data points to suitably

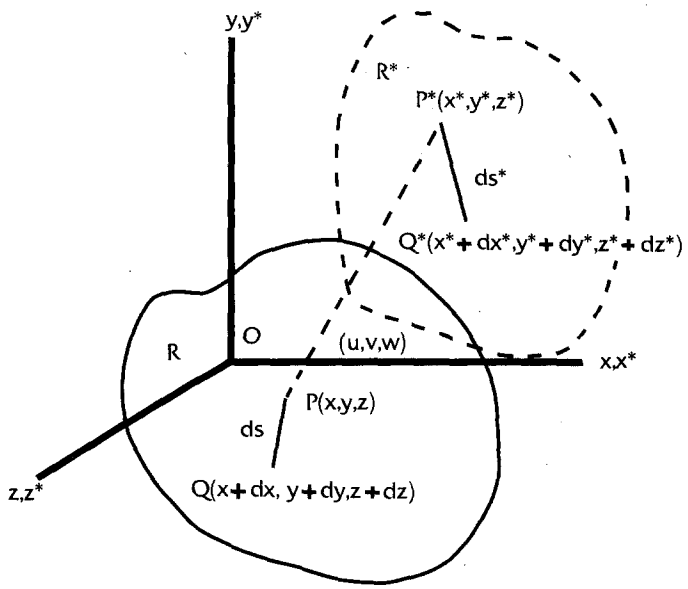

Fig. 2—Line segment PQ in undeformed and deformed bodies

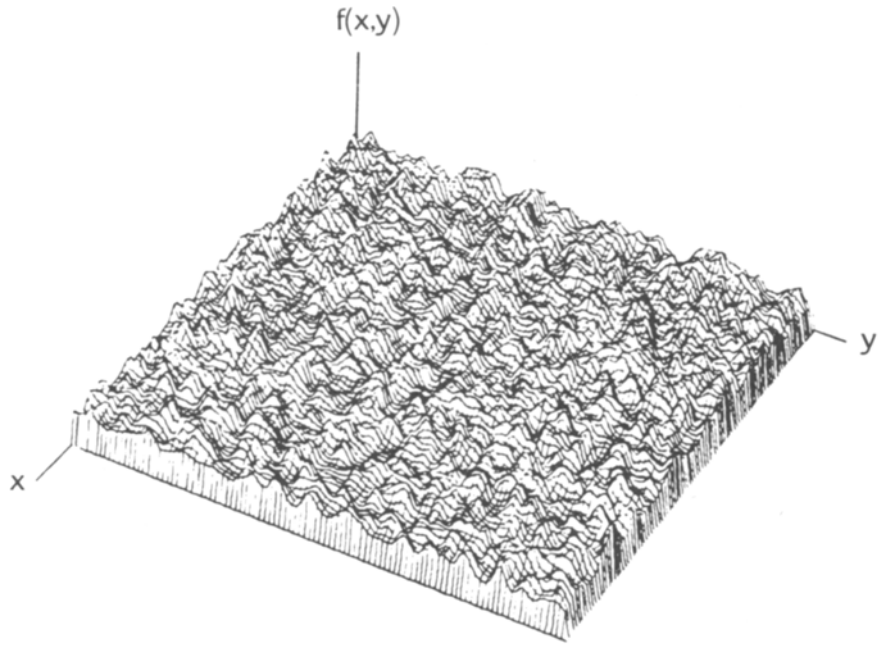

Fig. 3—Graphic representation of a digital-speckle image

reconstruct a continuous intensity pattern. (One should note that the frequency content of the data is not increased by interpolation.) A basic assumption that is obviously required for suitable reconstruction is that 'oversampling' of our intensity patterns, via the digitizing camera, is performed. For this to be true, one must limit the spatial-frequency content of the image so that oversampling is possible.[16-18]

Given the above assumptions, one may use several methods to fit surfaces to the data.[16,17] The surfaces used in this work were: (a) bilinear interpolation and (b) polynomial interpolation. Figure 6 portrays a 10 × 10 array of intensity data as it appears after fitting a bilinear surface to each and every square array of four data points. Figure 7 portrays a 30 × 30 array as it is represented by a tenth-order polynomial. Note that the polynomial surface smooths the data much more than the bilinear surface fit, thereby reducing the frequency content.

By using one of the methods noted above, two reconstructed image-plane intensity patterns are obtained.

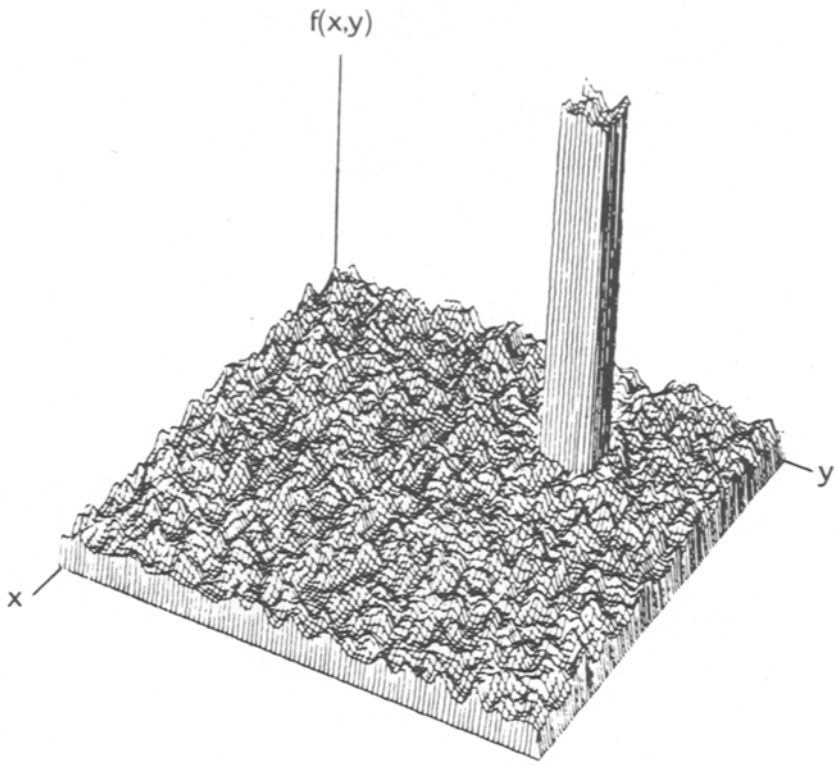

Fig. 4—Subimage surrounding point of interest P_0 (30,70) with size 10 × 10 pixels

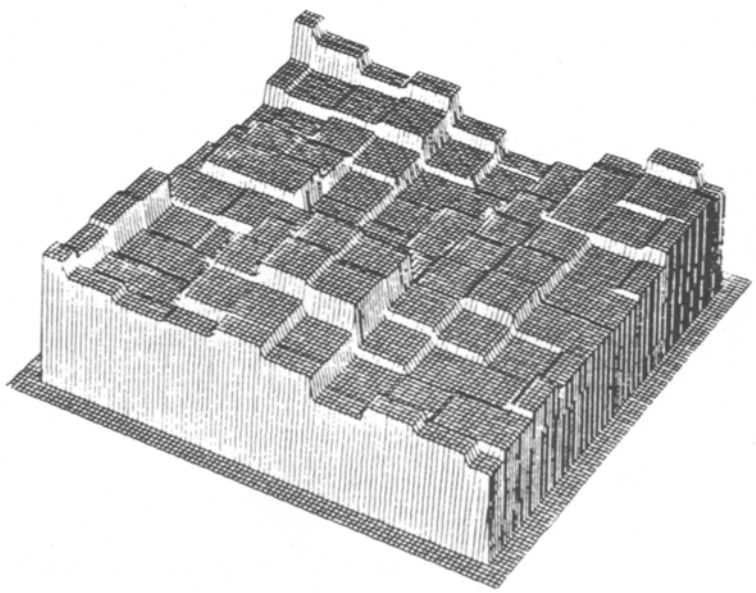

Fig. 5—Nearest neighbor interpolation (zero order)

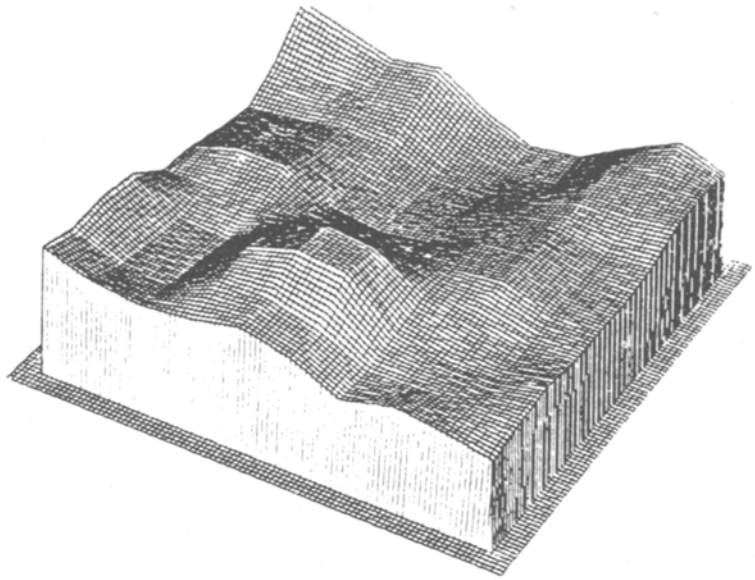

Fig. 6—Bilinear interpolation (first order)

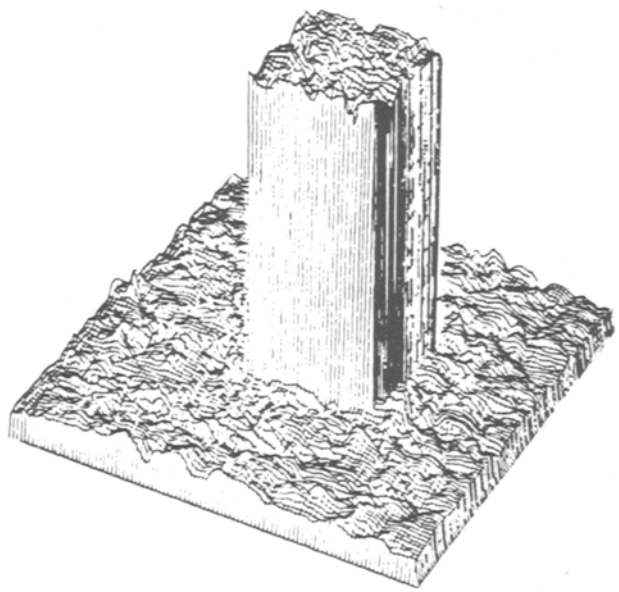

Fig. 7—30 × 30 subimage in the reference configuration fitted by a polynomial of degree 10

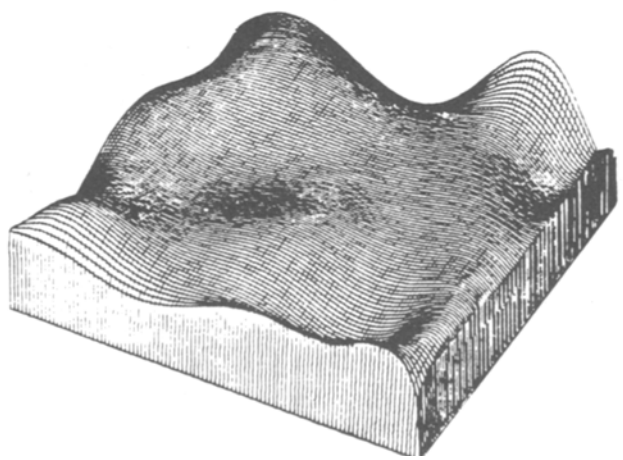

One surface represents the undeformed object and the other surface represents the deformed object. The image-correlation procedure, as discussed in the following section, uses the previous deformation analysis to compare local subsets of the undeformed intensity surface to those of the deformed intensity surface and thereby obtain the quantities of interest, which are displacement and strain.

Numerical Procedure for Deformation Analysis Using Digital-Image Correlation

Background

Consider a small subset of the object centered at P before deformation, as shown in Fig. 8. After deformation, the subset center moves to a new point P* and the subset deforms. If one uses the deformation assumption described previously, one can write the intensity values at positions P and P* as:

$$f(\mathrm{P}) = f(x, y)$$

$$f^*(\mathrm{P}^*) = f^*[x + u(\mathrm{P}), y + v(\mathrm{P})] \tag{8}$$

Similarly, for a point Q at position $(x + dx, y + dy)$ on the object prior to deformation, one can write the intensity values at positions Q and Q* by:

$$f(\mathrm{Q}) = f(x + dx, y + dy)$$

$$f^*(\mathrm{Q}^*) = f^*[x + u(\mathrm{Q}) + dx, y + v(\mathrm{Q}) + dy] \tag{9}$$

Finally, if one assumes that $f(\mathrm{Q}) = f^*(\mathrm{Q}^*)$ (i.e., that the intensity pattern deforms but does not alter its local value due to deformation) one has:

$$f(\mathrm{P}) = f[x + u(\mathrm{P}), y + v(\mathrm{P})]$$

$$f(\mathrm{Q}) = f[x + u(\mathrm{Q}) + dx, y + v(Q) + dy] \tag{10}$$

Figure 9 shows a small subset on the object surface centered at P, together with its deformed shape centered at P*. If one assumes that the subset is sufficiently small that straight lines remain straight after deformation, then one may use eqs (4) and (5) to describe the position of point Q* as:

$$(x^{**}, y^{**}) = (x^* + dx^*, y^* + dy^*)$$

$$[x + u(\mathrm{P}) + dx^*, y + v(\mathrm{P}) + dy^*] \tag{11}$$

$$= \left[x + u(\mathrm{P}) + \frac{\partial u}{\partial x}dx + \frac{\partial u}{\partial y}dy + dx,\right.$$

$$\left. y + v(\mathrm{P}) + \frac{\partial v}{\partial x}dx + \frac{\partial v}{\partial y}dy + dy\right]$$

Using eq (4), eq (10) can be rewritten as:

$$f^*[Q^*] = f\left[x + u(\mathrm{P}) + \frac{\partial u}{\partial x}(\mathrm{P})dx + \frac{\partial u}{\partial y}(\mathrm{P})dy + dx,\right.$$

$$\left. y + v(\mathrm{P}) + \frac{\partial v}{\partial x}(\mathrm{P})dx + \frac{\partial v}{\partial y}(\mathrm{P})dy + dy\right] \tag{12}$$

Thus, if one knows the displacement of the center point P of a subset and if one obtains the derivative terms $\frac{\partial u}{\partial x}(\mathrm{P})$, $\frac{\partial u}{\partial y}(\mathrm{P})$, then the position of any nearby point Q* is determined. Conversely, if one assumes values for $u(\mathrm{P})$, $v(\mathrm{P})$, $\frac{\partial u}{\partial x}(\mathrm{P})$, $\frac{\partial u}{\partial y}(\mathrm{P})$, $\frac{\partial v}{\partial x}(\mathrm{P})$, and $\frac{\partial v}{\partial y}(\mathrm{P})$, then one can compute estimates for the positions of points P* and all points Q* that are within the small subset surrounding P*. This latter statement forms the foundations for the numerical computation of local deformation.

Iterative Method

To obtain accurate values for the six variables of interest for any subset, one must in some sense compare subsets of the intensity pattern. Though the procedure for comparing subsets is discussed in Ref. 13, the method is summarized in the following paragraphs.

To start the analysis, a subset from the digitized intensity pattern of the undeformed object surface centered at

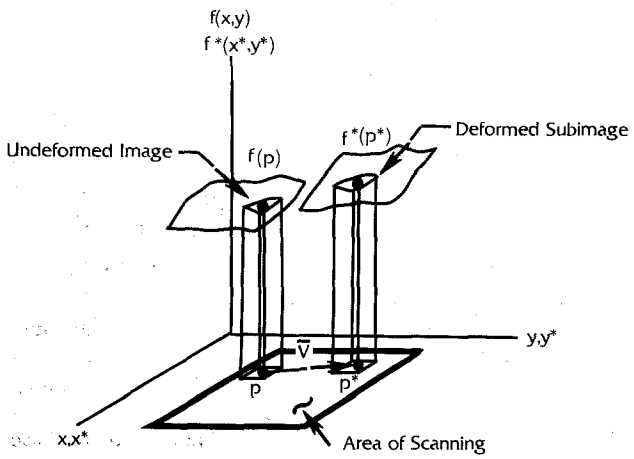

Fig. 8—Local motion and distortion of a subset image

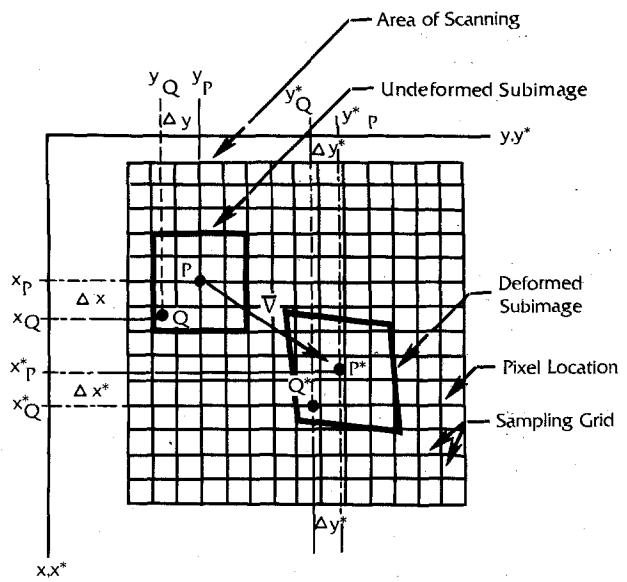

Fig. 9—Deformation of a subimage in a sampling grid

P is chosen. It is interpolated by one of the methods noted previously. Next, ranges on the values for displacements (u,v) of the subset center are chosen with the remaining variables set to zero. The undeformed subset intensity values $f(x,y)$ at selected points within the subset are then 'compared' to the intensity values $f^*(x^*,y^*)$ at positions $x^* = x+u$, $y^* = y+v$, as if the subset only translated without distortion. The values of u and v which give the best comparison is our approximate center point translation so that $[u(\mathrm{P}),\ v(\mathrm{P})] \cong (u_1, v_1)$. The method for comparing two subsets is commonly given by use of the cross-correlation coefficient, C,

$$C\left(u,v,\frac{\partial u}{\partial x},\frac{\partial u}{\partial y},\frac{\partial v}{\partial x},\frac{\partial v}{\partial y}\right) = \frac{\int_{\Delta M^*} f(x,y)\, f^*(x+\xi, y+\eta)\, dA}{\left[\int_{\Delta M}[(f(x,y)]^2\, dA \int_{\Delta M^*}[f^*(x+\xi,y+\eta)]^2 dA\right]^{1/2}}$$

where ΔM = subset in undeformed image, ΔM^* = subset in deformed image

$$\xi = u + \frac{\partial u}{\partial x}\Delta x + \frac{\partial u}{\partial y}\Delta y$$

$$\eta = v + \frac{\partial v}{\partial x}\Delta x + \frac{\partial v}{\partial y}\Delta y$$

The values of u, v, $\frac{\partial u}{\partial x}$, $\frac{\partial u}{\partial y}$, $\frac{\partial v}{\partial x}$, and $\frac{\partial v}{\partial y}$ which maximize C are the local deformation values for a subset. In any case, only (u,v) are assumed to vary; then the values of (u_1,v_1) computed by maximizing eq (13) on a subset are our first approximations for the translation of point P. Next, the ranges for the variables $\frac{\partial u}{\partial x}$, $\frac{\partial v}{\partial y}$ are chosen with u, v held fixed as (u_1,v_1) and $\frac{\partial u}{\partial y}$, $\frac{\partial v}{\partial x}$ are held at zero. The same iterative procedure used to compute u and v is repeated to give an estimate of the image-dilatation terms, $(\frac{\partial u}{\partial x})_1$ $(\frac{\partial v}{\partial y})_1$. Finally, ranges for $\frac{\partial u}{\partial y}$ and $\frac{\partial v}{\partial x}$ are chosen and the subsets are compared [with u_1, v_1, $(\frac{\partial u}{\partial x})_1$ and $(\frac{\partial v}{\partial y})_1$ all held constant] via eq (13) to give the first estimates, $(\frac{\partial u}{\partial y})_1$ and $(\frac{\partial v}{\partial x})_1$.

The entire procedure is then repeated with smaller ranges of values for u,v chosen around (u_1,v_1) and the other variables held constant. This 'two-parameter' system for iterating a solution continues until the difference in values for each variable is less than a specified error. The converged values for all six variables are then printed out. A new subset is then chosen and the procedure outlined above is repeated until all subsets of interest have been analyzed. As a final note, it should be clear to the numerical analyst that this 'two-parameter' iterative technique will not converge to the exact answers unless the problem is linear; the problem as stated is highly nonlinear due to the square root noted in eq (13). Improved algorithms are possible[20]; however, the algorithm just discussed has been used successfully by the authors in all of their applications.

Experimental Examples

A computer program known as STRAIN has been written to analyze the deformation of small subsets by use of two images. The procedure employed in STRAIN is described in the preceding section. In order to determine the utility of the proposed method, four experiments were performed. They are: (1) uniform translation (2) rigid-body rotation (3) constant angular velocity and (4) uniform finite strain. Together, these four experiments illustrate how the six deformation variables in eq (13) can be computed to determine the quantities of interest.

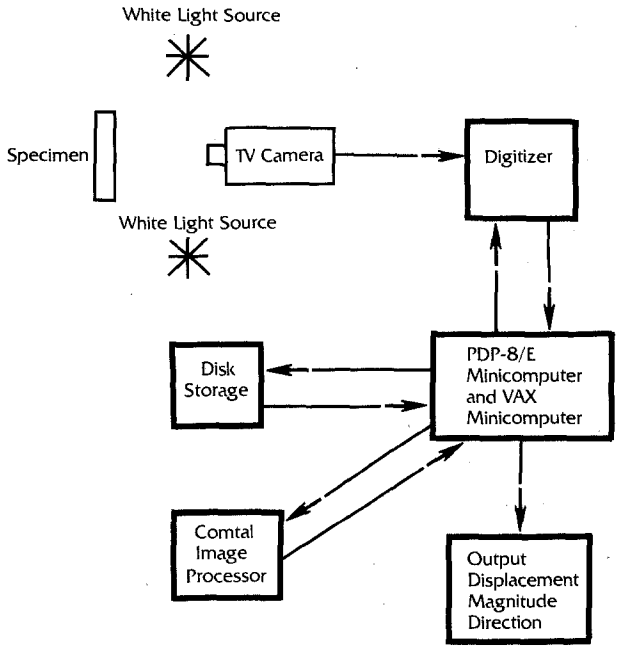

Fig. 10—Schematic of experimental configuration for correlation analysis

For each experiment, a data-acquisition system such as the one shown in Fig. 10 was used. It is noted that illumination to obtain laser speckle has been used for some situations. However, the results have not been as consistent as those obtained with white-light speckle. The reasons for this appear to be twofold. First, the laser speckles are quite small; usually the ratio of speckles to pixels is 5:1. Hence oversampling is not possible. Secondly, due to the coherent nature of the speckles, decorrelation of the speckles occurs when the surface incurs relatively small strains and/or rotations.

Uniform Translation

Two specimens were selected for uniform translation tests using the correlation method. An aluminum block with dimensions 50.8 × 38.1 × 6.35 mm was used as Specimen 1. One side of this specimen was treated to form a very rough surface, and was spray painted with flat white paint to scatter the laser light in order to generate a speckle pattern. Specimen 2 was 97.8 × 57.15-mm black cardboard lightly sprayed with white paint to form a random pattern as illustrated in Fig. 11.

An X-Y translation table was used to translate and position specimens. The table can take single steps of size .02032 mm between points with a repositioning accuracy of 0.00254 mm. A dial indicator with .0254-mm precision and a 5.08-mm range was clamped to the base of the table in order to measure the displacement of the table.

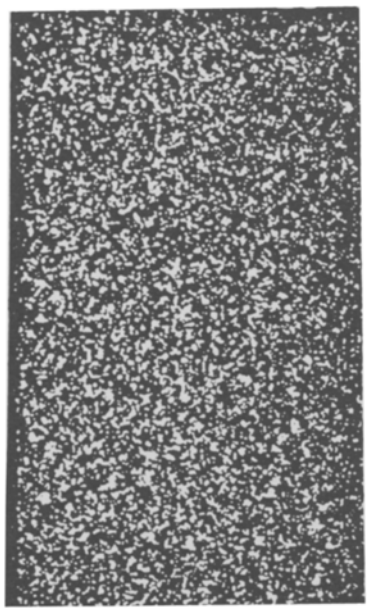

Fig. 11—Random pattern of whites speckles—Specimen 2

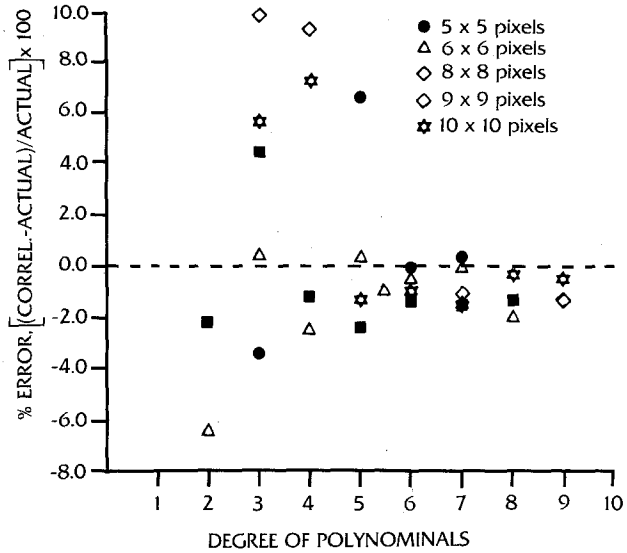

Fig. 12—Errors of correlated displacements using polynomial-fit method for actual displacement of 0.8026 mm for Specimen 1

In the first test, the aluminum specimen was firmly attached to the surface of the translation table, and was illuminated by a Spectra-Physics He-Ne cw laser to form a speckle pattern. The light from the laser was spatially filtered using a Spectra-Physics Model 332 spatial filter. The table was carefully aligned so that its line of movement was parallel to a horizontal line on the display screen of a monitor. After focusing the camera, the aperture and the speed of the scanner were adjusted to the desired setting. Next, the laser speckle pattern of the specimen was digitized and stored in the computer. The specimen was then displaced to a new position and the speckle pattern was digitized again. The pair of digital images recorded in the computer, corresponding to positions both before and after displacement, were analyzed later by the correlation method. The experimental procedure was similar for obtaining digital-image pairs of the second specimen. The cardboard with the white speckle pattern was attached to the X-Y table which has the micrometer indicators. Instead of using laser light, a uniform white-light field was used to illuminate the second test specimen.

For these cases, all gradients of displacement terms were held fixed at zero and the displacement of the subset was computed using the STRAIN program. Subset image resolution was 6.22 pixels per mm for each test. Errors of correlation with polynomial fit for various subimage sizes and different degrees of polynomials are shown in Fig. 12. For images fitted by polynomials, the CPU time required for correlation with higher degree polynomial fit is considerably longer than that with lower degree polynomial fit. For example, if 9 × 9 pixel subimages are fitted by polynomials of degree 7, then the CPU time required for the correlation of these subimages is 45 s. If polynomials of degree 3 are used, the CPU time required is only 2 s.

Correlated displacements calculated by the bilinear interpolation method are compared with the actual displacements in Fig. 13. The results using the bilinear-interpolation method are more accurate than those using

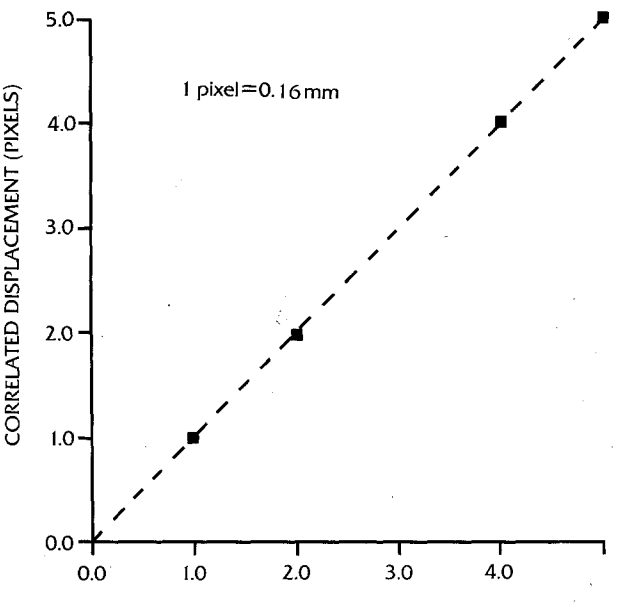

Fig. 13—Correlated displacements vs. actual displacements for Specimen 1 using bilinear interpolation method

the polynomial-fit method. The maximum CPU time used for correlation is only 5 s when the bilinear method is used.

Specimen 2 was used in several uniform translation tests for objects that had a white speckle pattern on the surface. The main objective of these tests was to verify the feasibility of the digital-image-correlation method in the determination of small displacements (less than 1 pixel).

Figure 14 shows the results from the correlation routines for a uniform translation test. The test was run with translations of .2, .4, .6, .8 and 1.0 pixels, one pixel

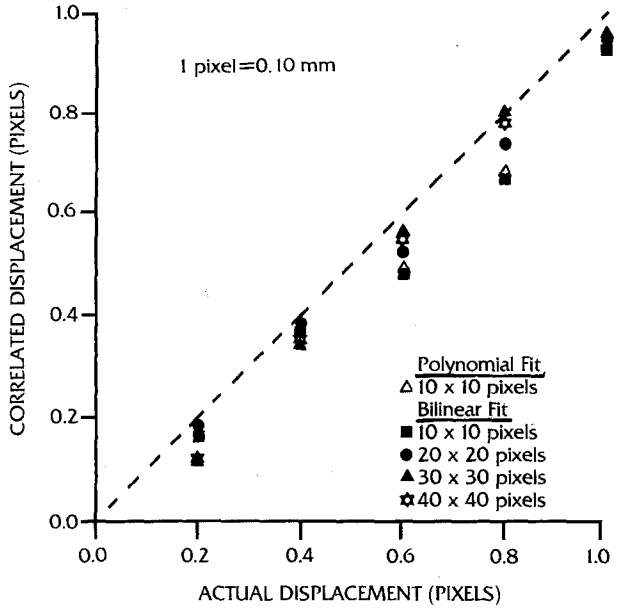

Fig. 14—Results for small uniform translation in Y direction—Specimen 2, Test 1

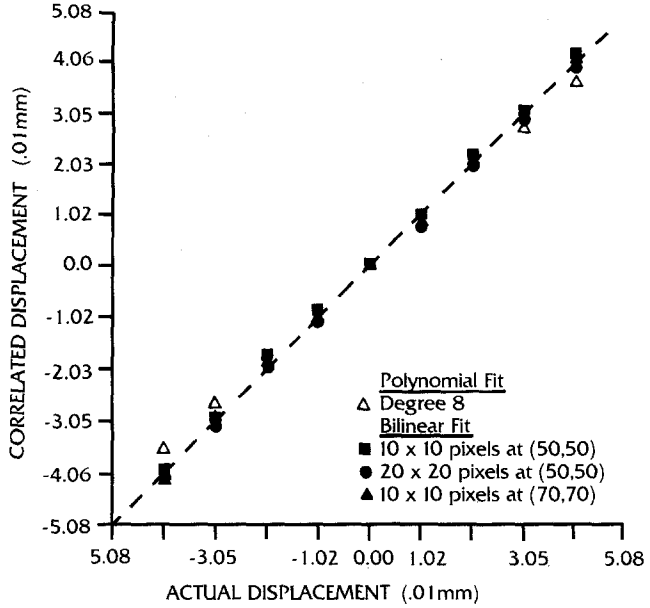

Fig. 15—Results for small uniform translation in Y direction—Specimen 2, Test 2

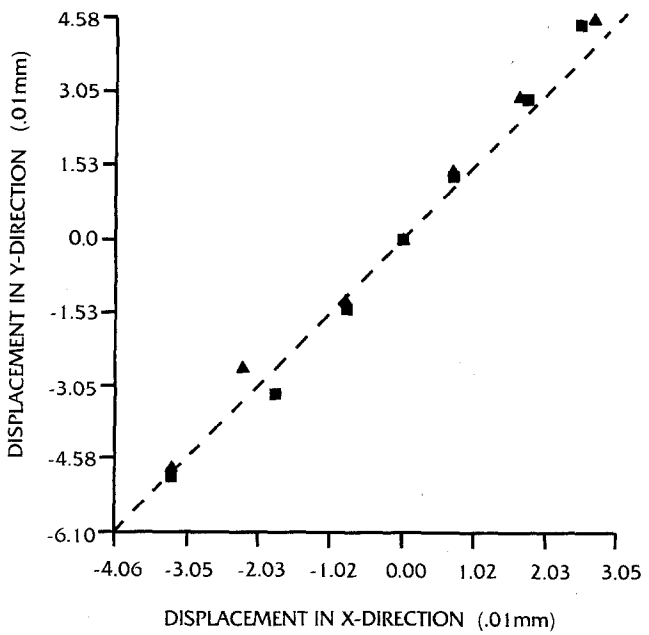

Fig. 16—Results for small uniform translation in X and Y directions

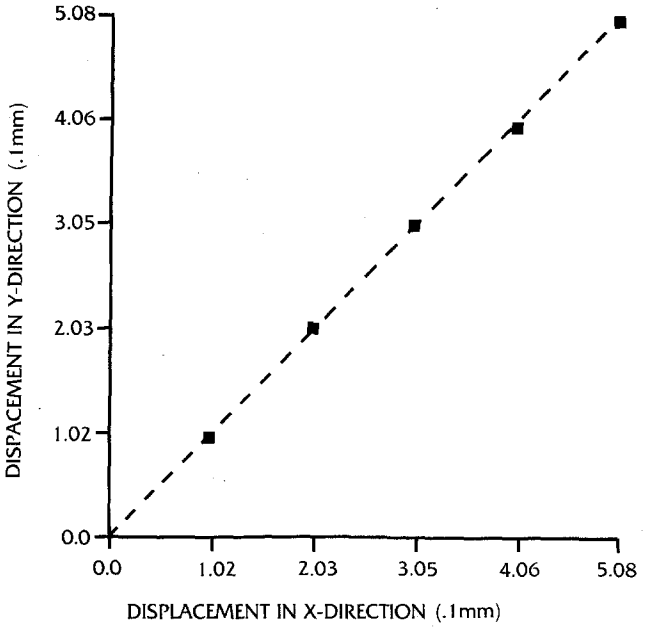

Fig. 17—Results for large uniform translation in X and Y directions

being .0991 mm of actual displacement. Both polynomial fit and bilinear-interpolation methods were used to represent the intensity patterns, as noted in Fig. 14. Results of a similar test for small uniform translation are shown in Fig. 15. Again, the correlated displacements using bilinear interpolation method are more accurate than those using polynomial-fit method.

Correlated data for uniform translation in both the x and y directions simultaneously with small overall displacements of less than 1 pixel and large overall displacement of 0.508 mm are plotted in Figs. 16 and 17, respectively. The correlated displacement components are within reasonable accuracy.

Rigid-Body Rotation

In the case of planar rigid-body rotation about a fixed point, two methods may be used to calculate the angle of

TABLE 1—ANGLE OF ROTATION DETERMINED USING DEFORMATION GRADIENTS FOR VARIOUS SUBIMAGE LOCATIONS

Location (Pixels)		*Displacement (mm)		Deformation Gradients		$\frac{1}{2}\left(\frac{\partial v}{\partial x} - \frac{\partial u}{\partial y}\right)$	†Angle of Rotation (deg)
X	Y	u_o	v_o	$\partial v/\partial x$	$\partial u/\partial y$		
50	20	.248	−.228	0.0420	−0.0308	0.0364	2.08
50	40	.110	−.239	0.0334	−0.0275	0.0304	1.74
50	50	.054	−.217	0.0387	−0.0371	0.0379	2.17
50	60	.014	−.223	0.0385	−0.0252	0.0318	1.82

*Image resolution is 5.43 pixels/mm in Y-direction.
†Actual rotation is 2 deg ±0.08 deg (precision of rotation table is 0.08 deg).

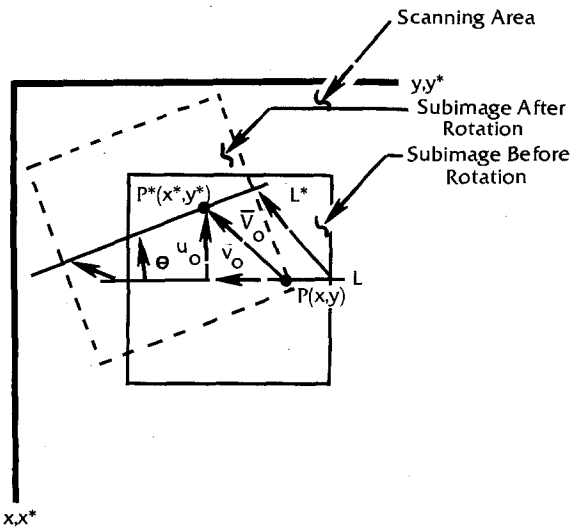

Fig. 18—Angle of rotation determined by displacement components

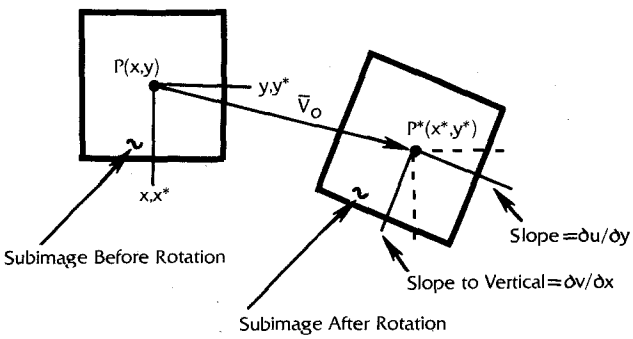

Fig. 19—Angle of rotation determined by deformation gradients

rotation based on the results from the correlation routines. First, the angle of rotation can be obtained by calculating the angle between an arbitrary line L in the reference image and its corresponding line L* after rotation in the deformed image as shown in Fig. 18. Suppose that the line L is parallel to the y axis and can be represented by $x = c$, where c is a constant. The coordinates of an arbitrary point on the line L after rotation can be determined by correlating the reference and the deformed images. By fitting a straight line over a number of points displaced from points on the line L, the line L* corresponding to the line L after rotation is obtained. Since L is parallel to the y axis, the angle between the lines L and L* may be calculated by the following equation.

$$\theta = \tan^{-1}(-m) \tag{14}$$

provided that the line L* is expressed in the form

$$x^* = my^* + b \tag{15}$$

where b is the intersection of L* with the x axis and m is the slope. Also, the rotation may be determined using the deformation terms directly. Consider a reference subimage at point P(x,y) as shown in Fig. 19. The displacement components and the four deformation gradients can be determined by correlating this subimage to the deformed image after rotation. For small rotations, commonly less than 10 deg, the angle of rotation, θ, may be approximated by use of eq (7):

$$\theta \cong \frac{1}{2}\left(\frac{\partial v}{\partial x} - \frac{\partial u}{\partial y}\right)$$

since the deformation gradients $\partial u/\partial x = \partial v/\partial y = 0$ and $\partial v/\partial x = -\partial u/\partial y$ theoretically.

Specimen 2 of the white speckle pattern was rotated by 2 deg counterclockwise in the first test. The image resolution of both images digitized before and after rotation was 5.43 pixels/mm. The least-squares interpolation method was used to fit the displacement data from 17 subsets corresponding to points on the center line parallel to the y axis. The line after rotation was then expressed in the following form:

$$x^* = 0.3059 - 0.03487\,y^* \tag{16}$$

and the angle of rotation was calculated by eq (16) as

$$\theta = \tan^{-1}(0.03487) = 1.997 \text{ deg}$$

The rotation determined by eq (16) using the deformation gradients is shown in Table 1 for several 20 × 20 pixel subimages in different locations.

TABLE 2—RESULTS OBTAINED USING DEFORMATION GRADIENTS FOR DIFFERENT ROTATIONS AND VARIOUS SUBIMAGE SIZES

*Actual Angle of Rotation (deg)	†Subimage Size (pixels)	Deformation Gradients		$\frac{1}{2}\left(\frac{\partial v}{\partial x} - \frac{\partial u}{\partial y}\right)$	Correlated Angle of Rotation (deg)	Error (percent)
		$\partial v/\partial x$	$\partial u/\partial y$			
3.0	20 × 20	0.0553	−0.0509	0.0531	3.04	1.3
4.0	20 × 20	0.0751	−0.0689	0.0721	4.12	3.0
5.0	20 × 20	0.0911	−0.0853	0.0882	5.02	0.4
6.0	20 × 20	0.1118	−0.1057	0.1088	6.23	3.8
6.0	10 × 10	0.1055	−0.1066	0.1060	6.05	0.8
6.0	15 × 15	0.1117	−0.1064	0.1090	6.22	3.7
6.0	20 × 20	0.1118	−0.1057	0.1088	6.23	3.8
6.0	30 × 30	0.1102	−0.1054	0.1078	6.15	2.5
6.0	40 × 40	0.1102	−0.1052	0.1077	6.14	2.4
6.0	50 × 50	0.1116	−0.1044	0.1080	6.16	2.7

*Precision of the rotation table is 0.08 deg.
†Image resolution is 6.457 pixels/mm in Y-direction.

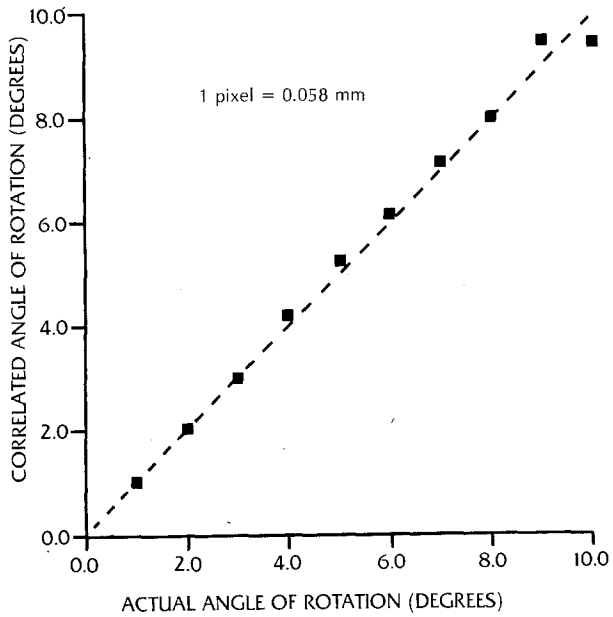

Fig. 20—Correlated rotation vs. actual rotation

A white speckle pattern similar to the one used on Specimen 2 was rotated by 3 deg, 4 deg, 5 deg, and 6 deg respectively. These images undergoing rotation were digitized with an image resolution of 6.4567 pixels/mm. The results obtained using the deformation gradient terms are shown in Table 2. The angles of rotation calculated by eq (16) are within reasonable accuracy. The effect of subimage size on the correlated angle of rotation is also shown in Table 2 for an actual angle of rotation of 6 deg. It shows that the size of the subimage has no significant effect on the results. Results obtained using the correlation method for a series of tests with overall rotation of 10 deg are plotted in Fig. 20. The correlated data does not agree with the actual value very well for rotations greater than 8 deg. These errors may be due to the linear approximation for the deformation of a subimage.

Constant Angular-Velocity Motion

The results from these experiments have been published previously[19] and are not reported here. However, the results indicate that the angular velocity of a body undergoing rotation about a fixed axis can be obtained with reasonable accuracy.

Uniform Finite-Strain Test

A simple load table was developed for the finite-strain test. As shown schematically in Fig. 21, an aluminum-alloy block was bolted to the base of the X–Y translation table. Two aluminum-alloy bars were used to clamp two ends of the specimen onto the translation and fixed tables, respectively. The specimen with its two ends clamped could be stretched a desired amount by simply moving the translation table away from the fixed table.

A thin rubber strip with dimensions 171.45 × 22.225 × 15.875 mm was used as the specimen. The specimen was lightly sprayed by white latex paint and was clamped at both ends. The unstretched length of the specimen between two clamps was measured as 97.028 mm. The experimental setup was aligned so that the center line of the specimen was approximately centered in the digitized image. A region near the fixed-end clamp was considered in this test to reduce the effect due to displacement. By moving the translation table away from the fixed table, a uniform traction is applied at the end sections of the rubber specimen. Figure 22 illustrates schematically the coordinate systems for the reference and deformed configurations of a subimage in the neighborhood surrounding a point of interest within the area of scanning. The images, before and after the specimen was stretched by an amount ΔL_y, were digitized. The displacement components as well as the deformation gradients at any point of interest were determined by the correlation of these two images.

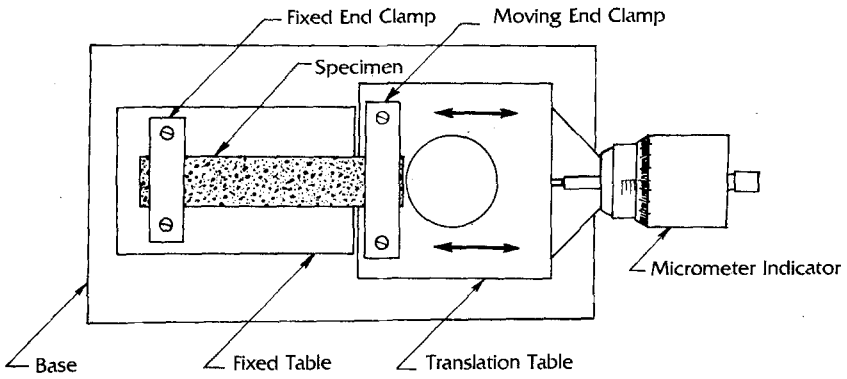

Fig. 21—Schematic drawing of load table with specimen

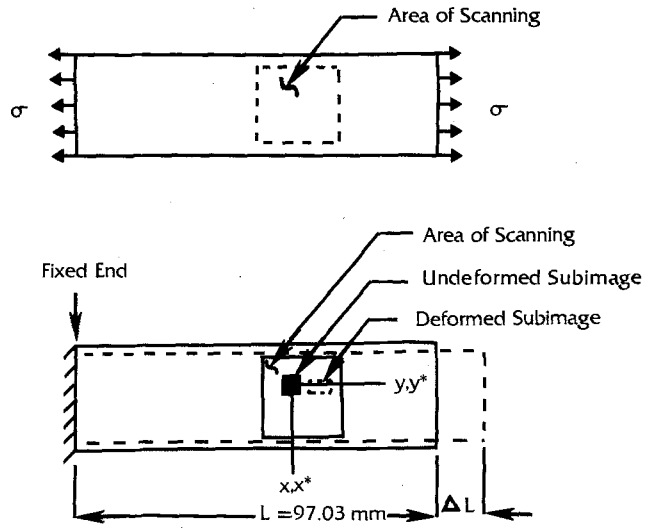

Fig. 22—Deformed and undeformed configuration of the rubber specimen

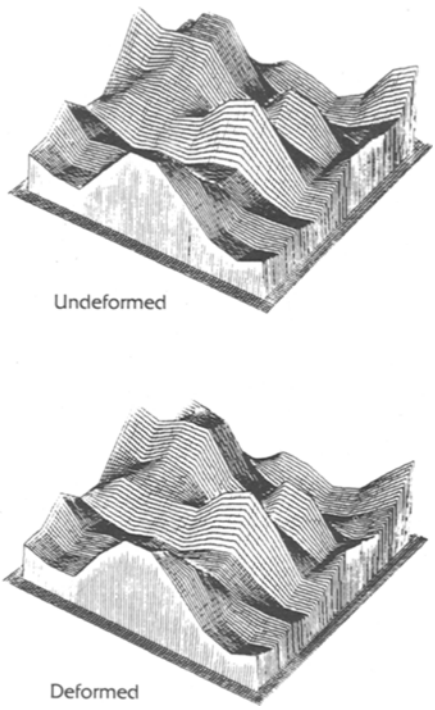

Fig. 23—Three-dimensional gray-level representation of subimage in the undeformed and deformed configurations for $\frac{\partial v}{\partial y} \cong \epsilon_y = 0.04$

Since a uniform traction is applied at the end sections of the isotropic homogeneous specimen with constant width, the strain components may be considered as uniform in the area of interest. Additionally, the deformation gradient term, $\frac{\partial v}{\partial y}$, can be approximated by

$$\frac{\partial v}{\partial y} \cong \frac{\Delta L_y}{L_y}$$

The gradient terms, $\frac{\partial u}{\partial y}$ and $\frac{\partial v}{\partial y}$, are negligibly small compared to the terms $\frac{\partial v}{\partial y}$ and $\frac{\partial u}{\partial x}$. Thus the finite-strain displacement relations defined by eq (6) may be rewritten as:

$$\epsilon_{xx} = \frac{\partial u}{\partial x} + \frac{1}{2}\left(\frac{\partial u}{\partial x}\right)^2$$

$$\epsilon_{yy} = \frac{\partial v}{\partial y} + \frac{1}{2}\left(\frac{\partial v}{\partial y}\right)^2$$

The specimen was first stretched with an overall elongation of 0.00598 mm for increments of 0.001496 mm. Thus the gradient term $\partial v/\partial y$, which is approximately equal to $\Delta L_y/L_y$, has a corresponding value ranging from 0.01 to 0.04. Figure 23 illustrates the three-dimensional gray-level representation of 11 × 11 pixel subimages before and after deformation for $\partial v/\partial y = 0.04$. The correlated data are tabulated in Table 3 for 30 × 30 subimages in different locations of the scanning area. It appears that the accuracy of the correlated data is higher for smaller displacement components of u. This is because the image distortion due to Poisson's effect is larger for locations having larger distance away from the center line of the specimen.

The results for the finite-strain test are plotted in Fig. 24. The correlated values of $\partial v/\partial y$ agree with the actual values within a reasonable accuracy (less than 10-percent error) for most of the data ranging from 0.01 to 0.03. Table 3 shows the results for the infinitesimal strain test ($\partial v/\partial y = 0.001$ and 0.002) with high image resolution (31.89 and 49.134 pixels/mm). The strain components,

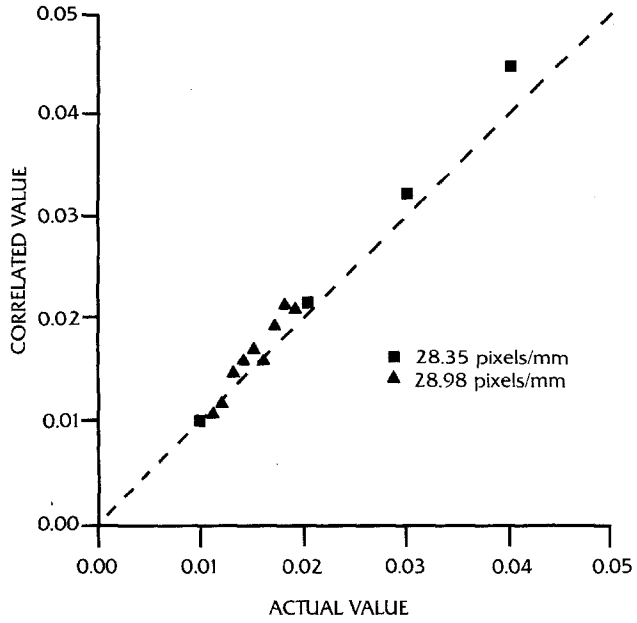

Fig. 24—Correlated data for finite-strain test

ϵ_{yy}, calculated by the correlation method are consistent for large image resolution (49.134 pixels/mm) and large subimage size of 50 × 50 pixels although the errors are not small (−18 to 8 percent). Since the load table is a spring-loaded device and may not be very accurate in measuring the displacement during the experiment, the instrument error may become significant for the small strain test.

It has been noticed that the deformation gradient terms, $\partial u/\partial x$ and $\frac{\partial v}{\partial y}$, are very sensitive to small changes in the minimum value of the correlation function during the iteration routines. The use of the higher order interpolation such as bicubic splines instead of the bilinear interpolation of the digital image may reduce the sensitivity of the gradient terms and, therefore, increase the accuracy of the results. However, the authors have not attempted to prove this hypothesis for the data presented in this section.

TABLE 3—NORMAL-STRAIN COMPONENT ϵ_{yy} DETERMINED BY CORRELATION METHOD FOR INFINITESIMAL STRAIN TEST

Subimage Size (pixels)	Image Resolution (pixels/mm)	Subimage Location (pixels)	*Actual Strain	*Correlated Strain	Error (percent)
30 × 30	31.9	70.50	0.001	0.00030	−70.0
30 × 30	31.9	50.50	0.001	0.00084	−16.0
30 × 30	31.9	30.50	0.001	0.00084	−16.0
30 × 30	49.13	70.50	0.001	0.00048	−52.0
30 × 30	49.13	30.50	0.001	−0.00036	−136.00
50 × 50	49.13	70.50	0.001	0.00108	8.0
50 × 50	49.13	50.50	0.001	0.00086	−14.0
50 × 50	49.13	30.50	0.001	0.00084	−16.0
50 × 50	49.13	70.30	0.002	0.00164	−18.0
50 × 50	49.13	50.50	0.002	0.00170	−15.0
50 × 50	49.13	30.50	0.002	0.00166	−17.0

*Strain component $\epsilon_{yy} = \partial v/\partial y$

Conclusions

The theory of the digital image-correlation method as used in experimental mechanics has been developed. A computer program based on this correlation method was developed for the determination of the displacement components and the deformation gradients of an object surface due to deformation. Several experiments were performed to demonstrate the viability of the correlation method in experimental mechanics.

The experimental results indicate that the correlation method is very accurate in the determination of rigid-body translations and rotations. In the uniform finite-strain test, the errors in the determination of the deformation gradient term were less than 10 percent for most of the $\partial v/\partial y$ values ranging from 0.01 to 0.03. The reduction of the errors may be accompanied by an increase in the image resolution. However, more work is necessary to determine the full range of deformation that can be measured by the digital-correlation method.

Acknowledgment

We wish to acknowledge the encouragement of C.J. Astill, the support of the National Science Foundation under grant #MEA 8214040 and the support of the National Institute of Health under grant #HL-27533.

References

1. Gabor, D., "A New Microscope Principle," Nature, **161**, 177-178 (1949).
2. Vest, C.M., Holographic Interferometry, Wiley and Sons (1979).
3. Leendertz, J.A., "Interferometric Displacement Measurement on Scattering Surfaces Utilizing Speckle Effect," J. Physics E: Scientific Inst., **3**, 214-218 (1970).
4. Archbold, E., Burch, J.M. and Ennos, A.E., "Recording on In-Plane Surface Displacement by Double Exposure Speckle Photography," Opt. Act., **17**, 883-898 (1970).
5. Archbold, E. and Ennos, A.E., "Displacement Measurement from Double-Exposure Laser Photographs," Ibid., **19**, 253-271 (1972).
6. Duffy, D.E., "Moiré Gauging of In-Plane Displacement Using Double Aperture Imaging," Appl. Opt., **11** (8), 1778-1781 (1982).
7. Hung, Y.Y., "A Speckle-Shearing Interferometer: A Tool for Measuring Derivatives of Surface Displacements," Opt. Comm., **11** (2), 132-135 (1974).
8. Chiang, F.P. and Asundi, A., "White Light Speckle Method of Experimental Strain Analysis," Appl. Opt., **18** (4), 409-411 (1979).
9. Durelli, A.J. and Parks, V.J., "Moiré Fringes as Parametric Curves," EXPERIMENTAL MECHANICS, **7** (3), 97-104 (March 1967).
10. Post, D., "Developments in Moiré Interferometry," Opt. Eng., **21** (3), 458-467 (1982).
11. Mendenhall, F.T., PhD Thesis, Theoretical and Appl. Mech. Dept., Univ. of Illinois (1981).
12. Peters, W.H. and Ranson, W.F., "Digital Imaging Techniques in Experimental Stress Analysis," Opt. Eng., **21** (3), 427-432 (1982).
13. Sutton, M.A., Wolters, W.J., Peters, W.H., Ranson, W.F. and McNeil, S.R., "Determination of Displacements Using an Improved Digital Correlation Method," Image and Vision Computing, **1** (3), 133-139 (1983).
14. Novozhilov, V.V., Theory of Elasticity, U.S. Dept. of Commerce Translation (1861).
15. Fung, Y.C., Foundations of Solid Mechanics, Prentice Hall Inc., Englewood Cliffs, NJ (1965).
16. Castleman, K.R., Digital Image Processing, Prentice Hall Inc., Englewood Cliffs, NJ (1979).
17. Andrews, H.C. and Patterson, C.L. III, "Digital Interpolation of Discrete Images," IEEE Trans. on Computers, V, C-25, (2) (Feb. 1976).
18. Tian, Qi and Huhns, M.N., "A Fast Hill Climbing Algorithm for Measuring Object Displacement with Sub-Pixel Accuracy," IEEE 12th Workshop on Applied Imagery Pattern Recognition, College Park, MD (Sept. 1983).
19. Peters, W.H., Ranson, W.F., Sutton, M.A., Chu, T.C. and Anderson, J., "Applications of Digital Correlation Methods to Rigid Body Mechanics," Opt. Eng., **22** (6), (Nov. 1983).
20. Dalloul, S.A., "Image Correlation in Deformable Bodies Including Non-Linear Geometries," PhD Thesis, Mech. Eng. Dept., Univ. of South Carolina (1984).